Noisy precursors and resonant properties of the period-doubling modes in a nonlinear dynamical system

Piotr Pierański and Jerzy Małecki
Institute of Molecular Physics, Polish Academy of Sciences, Smoluchowskiego 17/19, PL-60-179 Poznań, Poland
(Received 21 November 1985)

Response of the basic period-doubling mode of the dissipative Fermi-Ulam model to a periodic perturbation is studied both experimentally and theoretically. An intuitively obvious explanation of the noisy-precursors phenomenon is presented. Possible practical implications of the resonant-response phenomenon are discussed. Connections with the virtual Hopf phenomenon predicted by Wiesenfeld are indicated.

I. INTRODUCTION

This paper concerns a connection between two phenomena discovered recently in nonlinear dynamical systems: noisy precursors of period-doubling bifurcations and the resonant response of period-doubling modes.

As shown by Wiesenfeld,[1] random noise should induce new features in the power spectra of systems displaying stable periodic behavior as those systems approach a dynamical instability. In the case of a period-doubling instability the "new features" stand for broadband lines appearing in the power spectrum at the frequencies at which period doubling is to produce its next δ peaks. Such noise-induced lines, preluding the occurrence of a period-doubling instability, were observed in experiments on nonlinear *RLC* circuits.[2]

The second of the two phenomena mentioned above, the resonant response of period-doubling modes, was discovered in experiments on a nonlinear mechanical system.[3] Studying the bifurcation diagram of a basic, period-doubling mode of the system, we noticed that the phase of the mode responds to a periodic perturbation in a resonant manner. The peak of the resonant response proved to be dependent on the value of the nonlinearity parameter λ. For increasing λ the peak shifted within the response spectrum towards the frequency at which period doubling was to produce its next δ peak.

The noisy-precursors and resonant-response phenomena were discovered independently. It was not difficult to guess that in the case of period-doubling systems they might occur together and, if so, they should be closely connected. In the present paper we analyze quantitatively this connection reconsidering results of our previous experiments. Starting from an elementary theoretical description of the experimental system we show that the resonant-response phenomenon must, in the vicinity of a period-doubling bifurcation, result in the appearance of the Wiesenfeld's noisy precursor. The theoretical analysis is limited to systems whose dynamics can be described by the dissipative standard mapping. A general analysis of "... the sequence of events (as some parameter varies) whereby the noisy precursor of Hopf bifurcation continuously changes into the precursor of a period-doubling bifurcation" can be found in the latest Wiesenfeld paper.[4] In terms of his general theory the present paper provides the first experimental evidence for the "virtual Hopf phenomenon," as the defined above sequence of events is called, and gives a particular, experiment-based explanation of its origin. The resonant-response phenomenon we observed is an experimental manifestation of the virtual Hopf bifurcation he predicted.

The paper is organized as follows. In Sec. II we describe the physical system and results of experiments in which the resonant response of a period-doubling mode to periodic perturbation is shown to shift towards the frequency at which the period doubling is to produce its next δ peak. In Sec. III we present an elementary theoretical description of the experimental model and we analyze the resonant properties of its basic mode in the vicinity of the stability limits. Possible practical implications of the phenomenon and its connections with the general virtual Hopf phenomenon predicted by Wiesenfeld are discussed in Sec. IV.

II. PHYSICAL SYSTEM AND EXPERIMENTAL PROCEDURES

The experiments described below were performed on the jumping-particle model,[5] one of the simplest experimental systems which display the period-doubling transition from regular to chaotic motion. The model, a practical realization of the Fermi-Ulam idea,[6] consists of a particle (steel sphere) jumping vertically on a vibrating horizontal surface (glass plate fixed to the membrane of a loudspeaker); see Fig. 1. The surface vibrates sinusoidally at a constant audio frequency ν_0. The amplitude H of the vibration is precisely controlled by a helipot attenuator. The jumping particle can be seen as a strongly nonlinear oscillator driven at discrete moments of time by an external signal.

In the absence of the driving signal, i.e., when the collision surface stays still, the particle dropped on the surface will execute an infinite (theoretically) sequence of jumps. Because of the dissipation, a part $(0<k^2<1)$ of the particle kinetic energy is lost at each collision. Thus, the $(i+1)$th jump lasts $T_{i+1}=kT_i$, where T_i is the time length of the ith jump. Consequently, the $\{T_i\}_{i=1}^{i=\infty}$ sequence is geometrically convergent to zero and its sum,

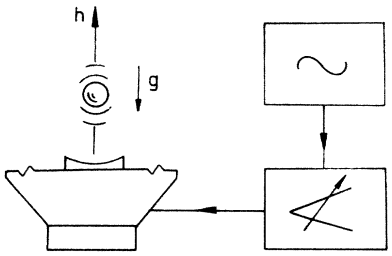

FIG. 1. Physical realization of the Fermi-Ulam model.

i.e., the total time duration of the jumping transient, is finite:

$$\sum_{i=1}^{\infty} T_i = T_1(1-k)^{-1} .$$

The sequence of jumps can be seen as a damped oscillation transient whose frequency $\nu(i) \sim 1/T_i$ diverges to infinity as $i \to \infty$. If, however, the collision surface is set by the external signal into sinusoidal motion, the particle can at a certain stage of the transient go into resonance with the surface and, compensating for losses of its energy at each collision, continue the motion in an endless sequence of jumps. Such a steady vibration of the system we shall refer to as "mode" in what follows.

From the whole variety of different modes which can be set within the experimental model[7] we consider below the simplest, denoted by $M^{(1)}$. In this mode the particle makes equidistant (in time) jumps between consecutive periods of the surface vibration function $h_s(t) = -H\cos(2\pi\nu_0 t)$. As seen from Fig. 2(a), where the mode is shown schematically, the collision moments t_i are always located at the same phase within the rising parts of the surface motion. Thus, at each collision, the losses of the particle kinetic energy are compensated via the momentum transfer from the collision surface moving upwards. Below a well-defined threshold H_0 of the surface vibration amplitude the $M^{(1)}$ mode ceases to exist since

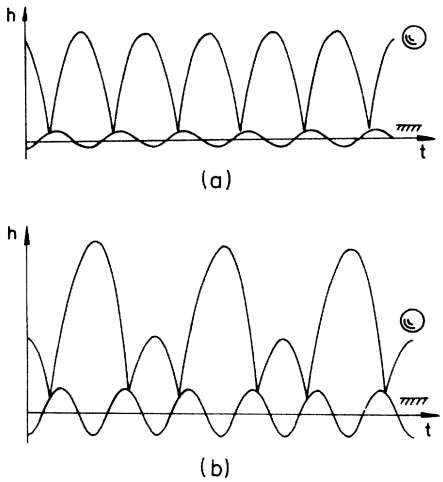

FIG. 2. Trajectories of the jumping particle in its (a) $M^{(1)}$ and (b) $M^{(1,2)}$ modes.

even at the phase at which the collision surface reaches its maximum velocity the losses of energy cannot be compensated. On the other hand, the $M^{(1)}$ mode becomes unstable when the amplitude of the surface vibration is too high, $H > H_1$, giving place to its period-doubled version $M^{(1,2)}$; see Fig. 2(b). The appearance of the $M^{(1,2)}$ mode completes the first stage of the theoretically infinite cascade of period doublings.

If at $H \in (H_0, H_1)$ the $M^{(1)}$ mode is perturbed, for example, by shifting the phase of the ith collision by Δ, then in the subsequent collisions the phase will return to its stationary value via a damped oscillatory transient. This suggests that the dynamics of the phase of the $M^{(1)}$ mode should be described in terms of a damped oscillator. To find the resonance frequency of the latter, one can either Fourier transform the transient or perform a typical stationary spectroscopy procedure, i.e., perturb the oscillator with a small-amplitude sinusoidal signal and monitor its response versus the slowly varying frequency of the latter. Such an experiment was performed by the present authors. The operational principle of the experimental setup we used, the details of which are described elsewhere,[3] is as follows.

The main signal driving the collision surface, i.e., the loudspeaker to whose membrane the glass plate is fixed, is either amplitude or frequency modulated by an additional signal of slowly increasing frequency ν. The response of the $M^{(1)}$ mode to the perturbation, i.e., deviations of the consecutive collision phases from their stationary position in the absence of the perturbation, is recorded versus ν with a storage oscilloscope.

Figure 3 presents typical images obtained by means of such a procedure at constant H and for a few different values of the amplitude of the perturbing signal. In view of the obvious relation between the envelopes of these images with recordings obtained from typical stationary spectroscopies, we shall in the following refer to the images as "spectra." As clearly seen in Fig. 3 the spectra display a characteristic resonance peak whose shape changes strongly with the amplitude of the perturbing signal; being smooth at low amplitudes, at higher amplitudes it becomes strongly deformed and reveals a rich internal structure. To avoid nonlinear effects, which are interesting on their own, in further experiments we kept the amplitude of the perturbing signal at a low value. In practice, the depth of the resulting modulation of the main signal was about 1%.

To obtain qualitative knowledge of how the resonant response of the $M^{(1)}$ mode changes along its bifurcation tree, we recorded its spectra at a number of amplitudes $H \in (H_0, H_1)$ of the main signal. The spectra were recorded both for the frequency modulation, Fig. 4, and amplitude modulation, Fig. 5. As seen from these figures, the spectra display a number of peaks located, in general, at frequencies

$$\nu_{\rm res}(H) \quad \text{and} \quad \nu_n^{\pm}(H) = n\nu_0 \pm \nu_{\rm res}(H), \quad n = 1,2,\ldots$$

where $\nu_{\rm res}(H) \in (0, \nu_0/2)$ denotes the location of the lowest-frequency peak. Since it is $\nu_{\rm res}(H)$ that determines the position of all peaks within the spectra, it was studied quantitatively by recording a series of precise FM spectra

within the relevant $(0,\nu_0/2)$ frequency range. The spectra were taken at a number of different points of the bifurcation tree including the branches of the period-doubled $M^{(1,2)}$ mode. All the spectra presented in Fig. 6 were taken at the same level of the perturbing signal. Although small enough to provide clear, smooth spectra for $H\in(H_0,H_1)$, i.e., the main single branch of the bifurcation tree, the perturbing signal proved to be too large for studies of the $M^{(1,2)}$ mode. As seen from Fig. 6 Z, Z', Z'', at the applied level of perturbation, the two branches of the $M^{(1,2)}$ mode became locally (in the vicinity of the resonance peaks) interconnected, i.e., the mode was practically destroyed. Let us note that the phenomenon occurs in a sudden, dischargelike manner as soon as the deviations of the phase from its stable position exceed a threshold value; the critical deviation is much smaller than the separation of the two branches themselves.

The frequency scale of the presented spectra can be easily determined from their internal structure. Namely, all points at which ν passes through a low-order commensurability with ν_0 are clearly distinguished by the characteristic stroboscopic patterns which appear in their vicinity.

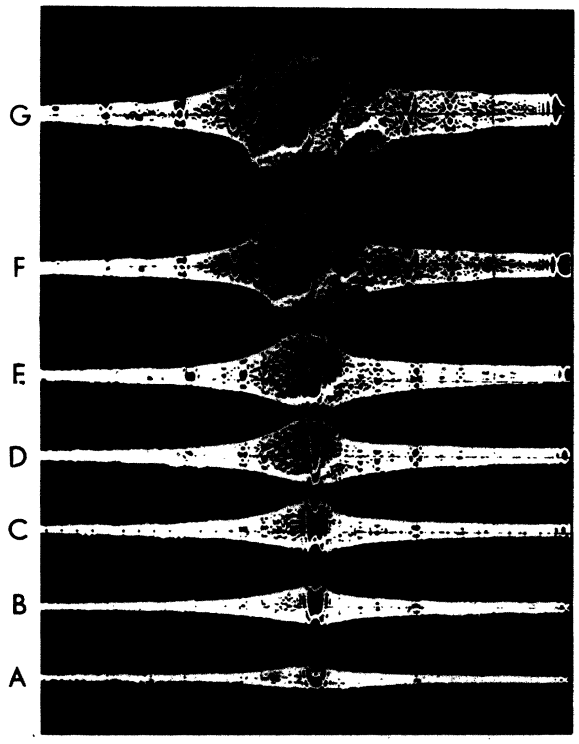

FIG. 3. Phase response spectra of the $M^{(1)}$ mode recorded for a few different amplitudes of the periodic perturbation. The amplitude H of the vibration of the collision surface determining the position of the $M^{(1)}$ mode within its bifurcation tree was the same for all presented spectra. Amplitudes of the perturbing signal were equal to 0.2, 0.3, 0.4, 0.5, 0.6, 0.75, and 1.0 for spectra denoted as $A,B,\ldots,G$. The frequency ν of the perturbing signal was swept linearly from about zero to $\nu_0/2$; $\nu_0=34$ Hz. The stroboscopic pattern of the $\frac{1}{3}$ commensurability point is clearly visible in the middle of the resonance peak.

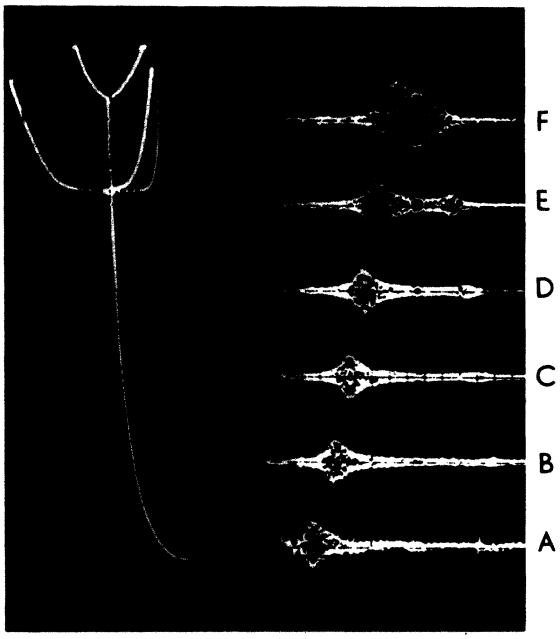

FIG. 4. Phase response FM spectra of the $M^{(1)}$ mode recorded at six points of its bifurcation tree (shown at the left side of the picture). The frequency ν of the perturbing signal was swept up to ν_0 (=33 Hz).

As seen in Fig. 6, $\nu_{res}(H)$ tends to 0 and $\nu_0/2$ for $H\rightarrow H_0^+$ and $H\rightarrow H_1^-$, respectively. Above H_1, where the single branch of the $M^{(1)}$ mode bifurcates into two branches of the period-doubled $M^{(1,2)}$ mode, two resonance peaks appear in the studied $(0,\nu_0/2)$ frequency range. If by $\nu_{res}(H)$ we denote once more the location of the lower peak, then the position of the upper peak can be specified as $\nu_1^-H=\nu_0/2-\nu_{res}(H)$. As H tends to H_2, i.e.,

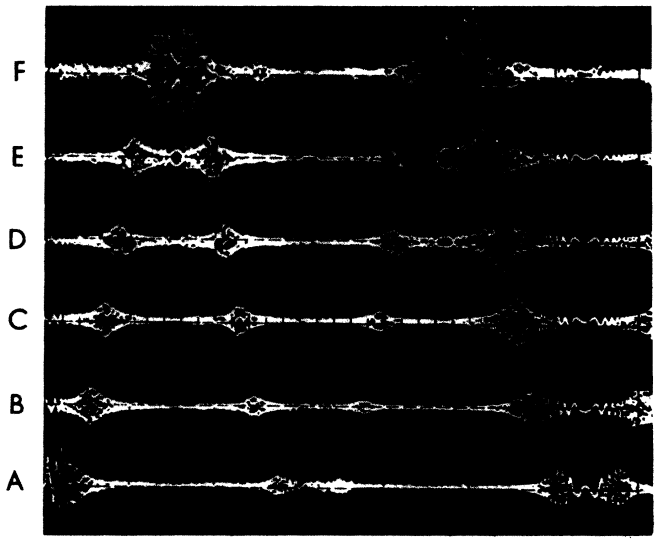

FIG. 5. Phase response AM spectra of the $M^{(1)}$ mode recorded at six points of its bifurcation tree (same as in Fig. 4). The frequency ν of the perturbing signal was swept up to $2\nu_0$ (=33 Hz).

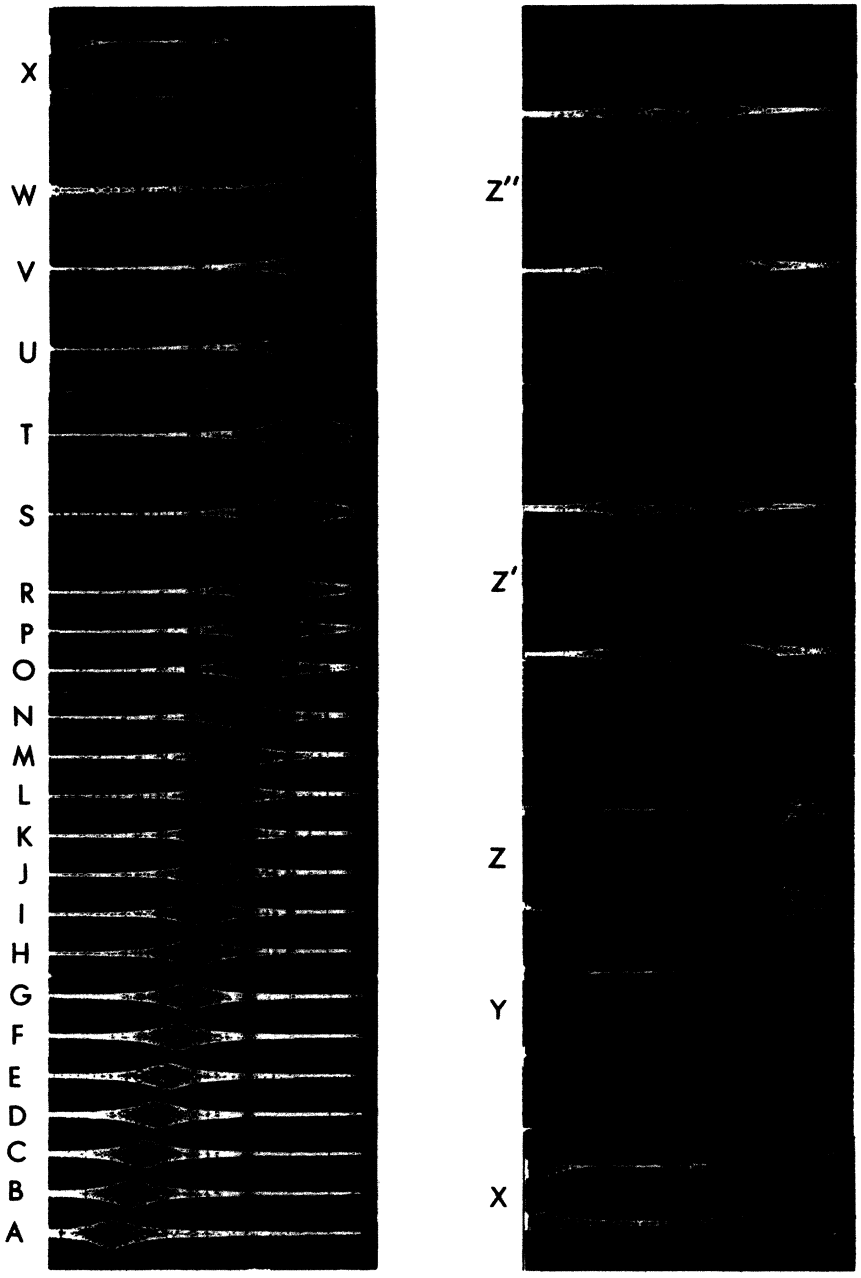

FIG. 6. Phase response FM spectra of the $M^{(1)}$ mode recorded at 27 points of its bifurcation tree including the $M^{(1,2)}$ period-doubled mode. In arbitrary units, in which $H_0=0.24$ and $H_1=1.00$, the positions of spectra indicated as $A,B,\ldots,Z,Z',Z''$ are, respectively, $H=0.28$, 0.32, 0.36, 0.39, 0.43, 0.46, 0.50, 0.54, 0.57, 0.61, 0.64, 0.68, 0.72, 0.75, 0.79, 0.82, 0.86, 0.90, 0.93, 0.97, 0.99, 1.00, 1.02, 1.04, 1.06, 1.15, 1.17. The frequency ν of the perturbing signal was swept up to $\nu_0/2$. A single frequency sweep lasted 100 s. $\nu_0=34$ Hz.

to the upper stability limit of the $M^{(1,2)}$ mode, $\nu_{\text{res}}(H)$ tends to $\nu_0/4$, while near the lower H_1 limit it tends to zero.

Resonant properties of the stable modes can also be studied using an alternative technique. Namely, one can keep both the amplitude and the frequency ν of the perturbing signal constant and sweep the amplitude H of the main signal, recording thus the image of the bifurcation tree in the presence of the periodic perturbation. Images obtained by means of such a technique are presented in Fig. 7.

III. THEORETICAL DESCRIPTION OF THE MODEL AND THE RESONANT-RESPONSE LINEAR APPROXIMATION

The experimental simplicity of the jumping-particle model results in the equally simple theory of its dynamics. As shown below, the theory can be built directly from the analysis of the consecutive collision events.

Let w_{i-1} be the velocity (in the laboratory reference frame) with which at time t_{i-1} the particle starts on its $(i-1)$st jump. At time $t_i=t_{i-1}+T_{i-1}$ the particle ar-

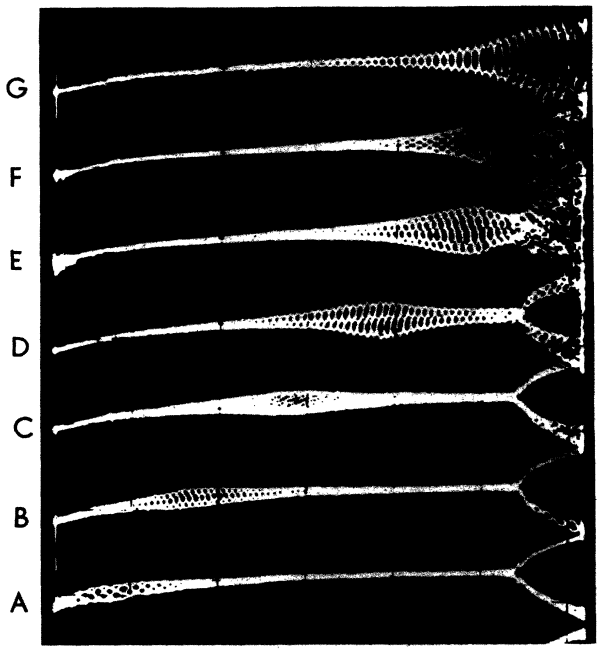

FIG. 7. Bifurcation tree of the $M^{(1)}$ mode recorded in the presence of a periodic perturbation. The frequency ν of the perturbing signal was equal to 20, 25, 30, 35, 40, 45, and 50 Hz for recordings marked, respectively, as $A,B,\ldots,G$. $\nu_0=100$ Hz.

rives back at the surface with velocity $w_{i-1}-gT_{i-1}$, where g is the gravitational acceleration constant. Thus, in the reference frame connected with the collision surface, its velocity equals $w_{i-1}-gT_{i-1}$ $-2\pi\nu_0 H\sin(2\pi\nu_0 t_i)$. Because of the dissipation, only a part $(0<k<1)$ of the relative velocity is reflected during the collision; thus, the velocity with which the particle starts on its ith jump equals

$$w_i=k(gT_{i-1}-W_{i-1})+(k+1)2\pi\nu_0 H\sin(2\pi\nu_0 t_i)\ . \tag{1}$$

The time length of the ith jump can be found from the condition

$$-H\cos(2\pi\nu_0 t_i)+w_i T_i-\tfrac{1}{2}gT_i^2=-H\cos[2\pi\nu_0(t_i+T_i)]\ , \tag{2}$$

which describes the $(i+1)$st collision event at which the particle trajectory [left-hand side of (2)] meets the trajectory of the collision surface [right-hand side of (2)]. Only those trajectories whose starting velocities w_i are larger than the respective surface velocities $-2\pi\nu_0 H\sin(2\pi\nu_0 t_i)$ and whose time lengths T_i are positive have a real physical sense. Equation (2) simplifies considerably in the case of all modes in which consecutive collisions take place at the same phase of the surface motion. For such modes, e.g., $M^{(1)}$, $T_i=2w_i/g$. Consequently,

$$t_{i+1}=t_i+2w_i/g\ . \tag{3}$$

Defining

$$\Theta=2\pi\nu_0 t \tag{4}$$

and

$$v=\frac{4\pi\nu_0}{g}w\ , \tag{5}$$

we transform (1) and (3) into the dimensionless form

$$v_i=kv_{i-1}+\lambda\sin\Theta_i\ , \tag{6a}$$

$$\Theta_{i+1}=\Theta_i+v_i\ , \tag{6b}$$

where

$$\lambda=\frac{(k+1)8\pi^2\nu_0^2}{g}H \tag{7}$$

plays the role of the nonlinearity parameter of the two-dimensional area-contracting (for $k<1$) mapping (6). In terms of Eq. (6) the angular frequency ω_0 of the surface vibration equals 1 and the Θ length of the particle jumps in the $M^{(1)}$ mode equals 2π. Consequently, the $M^{(1)}$ mode is described by

$$\Theta_i=\pi-\epsilon(\lambda)+i2\pi\ , \tag{8}$$

where $\epsilon(\lambda)$ denotes the shift of the collision moments Θ_i from the consecutive, negative-slope zeros of the surface action function $\lambda\sin\Theta$. The shift, previously discussed as necessary to compensate losses of the particle kinetic energy, can be determined from the balance condition

$$(1-k)2\pi=\lambda\sin[\pi-\epsilon(\lambda)]\ . \tag{9}$$

Thus

$$\epsilon(\lambda)=\arcsin\left[\frac{1-k}{\lambda}2\pi\right]\ . \tag{10}$$

Obviously, the shift cannot exceed $\pi/2$ since above this value the $\lambda\sin(\pi-\epsilon)$ term begins to decrease. This determines the lower stability limit for the $M^{(1)}$ mode:

$$\lambda_0=(1-k)2\pi\ . \tag{11}$$

The origin of the upper stability limit

$$\lambda_1=2[(1+k)^2+(1-k)^2\pi^2]^{1/2} \tag{12}$$

of the $M^{(1)}$ mode can be in intuitive terms explained as follows. The consecutive collisions are located in the $M^{(1)}$ mode at the negative-slope parts of the surface action function $\lambda\sin\Theta$. Thus, a deviation Δ in the location of a collision phase $\tilde{\Theta}_i=\Theta_i[\mathrm{mod}(2\pi)]$ from its proper $\pi-\epsilon(\lambda)$ place will be partially compensated in the next jump—the negative slope creates a negative feedback driving the $M^{(1)}$ mode phase back to its stable position. If, however, the slope is too high, which happens for $\lambda>\lambda_1$, the negative feedback overreacts by altering the next collision moment Θ_{i+1} by more than Δ to the other side of the $\pi-\epsilon(\lambda)$ location.

Concluding, for $\lambda\in(\lambda_0,\lambda_1)$ the $M^{(1)}$ mode is stable, and when perturbed it returns to its stationary phase $\pi-\epsilon(\lambda)$ via a damped oscillatory transient. Figure 8 presents shapes of such transients calculated numerically according to (6) for a few values of λ in the vicinity of λ_0 and λ_1.

Dynamics of the deviations

$$x_i=\tilde{\Theta}_i-\tilde{\Theta}^0\ , \tag{13a}$$

$$y_i=v_i-v^0 \tag{13b}$$

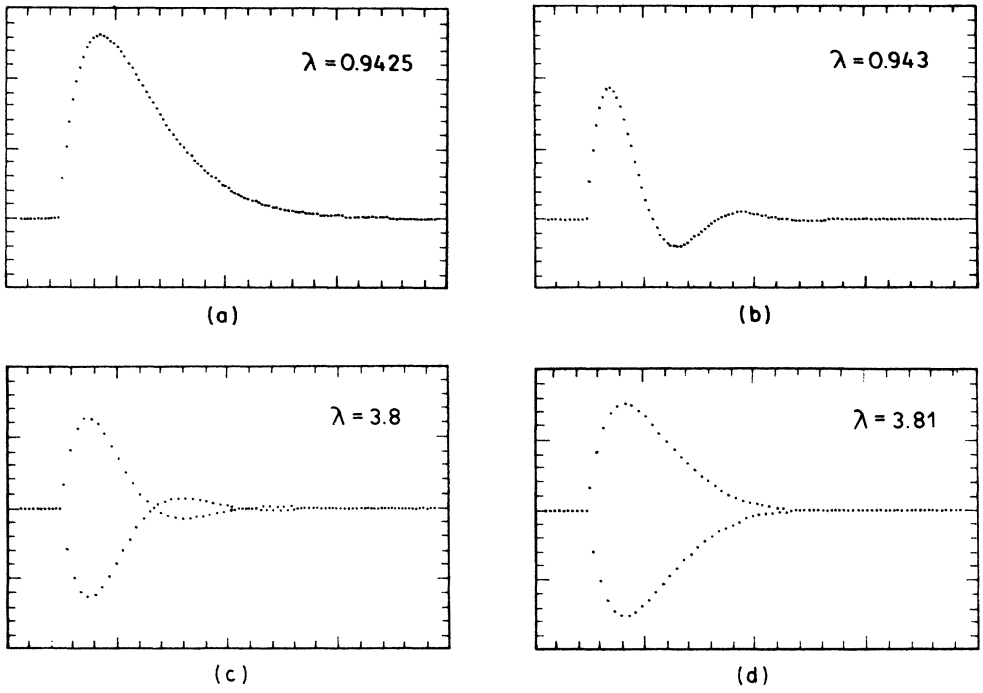

FIG. 8. Return transients of the $M^{(1)}$ mode phase $\tilde{\Theta}_i$ calculated according to (6) at different points of the bifurcation tree; $k=0.85$. The mode has been kicked out from its stable position by an instantaneous perturbation of its $v^0=2\pi$ velocity. (a) and (b) show the return transients near the $\lambda_0=0.942\,48$ lower stability limit, while (c) and (d) show such transients near the upper $\lambda_1=3.818\,15$ stability limit. One division of the $\tilde{\Theta}$ vertical scale equals $\pi\times10^{-5}$ and $1.66\pi\times10^{-5}$ for plots (a),(b) and (c),(d), respectively.

of the phase $\tilde{\Theta}_i=\Theta_i[\mathrm{mod}(2\pi)]$ and velocity v_i of the $M^{(1)}$ mode from their stationary $\tilde{\Theta}^0=\pi-\epsilon(\lambda)$ and $v^0=2\pi$ values is described by two first-order difference equations

$$y_i=ky_{i-1}-\lambda'\sin x_i\ , \tag{14a}$$

$$x_{i+1}=x_i+y_i\ , \tag{14b}$$

which are obtained by inserting (13) into (6). $\lambda'=\lambda\sin\tilde{\Theta}^0$ denotes the nonlinearity parameter of the new mapping. In view of (10), λ' can be expressed as

$$\lambda'(\lambda)=(\lambda^2-\lambda_0^2)^{1/2}\ . \tag{15}$$

In the vicinity of λ_0 and λ_1, λ' is well approximated by

$$\lambda'(\lambda_0+\epsilon)\cong(2\lambda_0)^{1/2}\epsilon^{1/2} \tag{16}$$

and

$$\lambda'(\lambda_1-\epsilon)\cong(\lambda_1^2-\lambda_0^2)^{1/2}-\lambda_1(\lambda_1^2-\lambda_0^2)^{-1/2}\epsilon\ , \tag{17}$$

where

$$\lambda_1^2-\lambda_0^2=2(k+1)\ .$$

Let us note that due to the minus sign at the $\lambda'\sin x_i$ term of Eq. (14a) the simplest stationary solution, i.e., point attractor of mapping (14), is located at $x=0$, $y=0$.

For $|x_i|\approx0$, Eq. (14a) can be linearized

$$y_i=ky_{i-1}-\lambda'x_i\ , \tag{18a}$$

$$x_{i+1}=x_i+y_i\ . \tag{18b}$$

The two first-order difference equations can be put together into one second-order equation

$$(x_{i+1}-2x_i+x_{i-1})+(1-k)(x_i-x_{i-1})+\lambda'x_i=0 \tag{19}$$

describing the discrete-time i dynamics of the deviations x_i of the $M^{(1)}$ mode phase from its stationary location. Since as seen from Figs. 8(a) and 8(b), for transients observed near λ_0, consecutive x_i's differ but by small amounts, the difference equation (19) can be replaced by its differential equivalent

$$\ddot{x}+2h_0\dot{x}+\omega_0^2x=0\ , \tag{20}$$

where

$$h_0=(4\pi)^{-1}(1-k) \tag{21}$$

and

$$\omega_0^2(\lambda)=(2\pi)^{-2}\lambda'(\lambda)\ . \tag{22}$$

$\ddot{x}$ and $\dot{x}$ denote here, respectively, the second and the first derivatives of x taken over the continuous variable Θ, which between two consecutive collisions changes on average by 2π. Equation (20) describes the dynamics of a conventional damped harmonic oscillator whose characteristic frequency ω_0 decreases rapidly as $\lambda\to\lambda_0$,

$$\omega_0(\lambda+\epsilon)\cong(2\pi)^{-1}(2\lambda_0)^{1/4}\epsilon^{1/4} \tag{23}$$

but whose damping factor h_0 stays constant. Consequently, the amplitude $A(\omega,\lambda)$ of its response to a periodic perturbation of frequency ω

$$A(\omega,\lambda)=c_0\{[\omega_0^2(\lambda)-\omega^2]^2+4h_0^2\omega^2\}^{-1/2} \tag{24}$$

changes strongly near λ_0, where $h_0\omega_0^{-1}(\lambda)\to\infty$. Figure 9 presents shapes of $A(\omega,\lambda)$ calculated according to (24), (22), (21), and (15) for a few values of λ in the vicinity of λ_0. The calculations were made for $k=0.85$ which fits well the experimental data of Fig. 6. As seen from Fig. 9 the resonance peak of $A(\omega,\lambda)$ located at

$$\omega_{\rm res}(\lambda)=[\omega_0^2(\lambda)-2h_0^2]^{1/2} \tag{25}$$

shifts with decreasing λ towards zero and reaches the limit value in a critical manner at a $\lambda_0^*>\lambda_0$ determined by

$$\omega_0(\lambda_0^*)=2^{1/2}h_0\ . \tag{26}$$

Thus, for $\lambda\in(\lambda_0,\lambda_0^*)$ we observe in $A(\omega,\lambda)$ a single peak located at $\omega=0$.[8] It is essential to be aware that this happens not due to an increase of the damping factor h_0 but due to the decrease of the characteristic frequency $\omega_0(\lambda)$. Using more intuitive terms we may say that the parabolic well, within which the phase of the $M^{(1)}$ mode is locked, flattens rapidly near λ_0. Since $A(0,\lambda)$ has the physical sense of an oscillator response to a constant force, this flattening of the potential well results in the divergence of $A(0,\lambda)$ for $\lambda\to\lambda_0$:

$$A(0,\lambda_0+\epsilon)=C_0(2\pi)^2(2\lambda_0)^{-1/2}\epsilon^{-1/2}\ . \tag{27}$$

Concluding, near λ_0 the phase of the $M^{(1)}$ mode becomes extremely sensitive to low-frequency perturbations. This phenomenon is accompanied by the divergence of the relaxation time τ. Namely, for λ such that $\omega_0(\lambda)<h_0$ the oscillator (20) becomes overdamped and its relaxation time diverges according to the power law

$$\tau(\lambda_0+\epsilon)=(1-k)(2\pi)^{-1}(2\lambda_0)^{-1/2}\epsilon^{-1/2}\ . \tag{28}$$

A similar analysis can be performed near λ_1. Namely, in the vicinity of this instability point, consecutive x_i's are almost exactly opposite, i.e., every other x_i changes but by a small amount. [See Figs. 8(c) and 8(d).] This suggests the possibility of formulating an equation analogous to (20). Indeed, using (18) one can obtain

$$(x_{i+4}-2x_{i+2}+x_i)+(1-k^2)(x_{i+2}-x_i)+[2(k+1)-\lambda']\lambda' x_i=0\ . \tag{29}$$

Since near λ_1 differences between every other x_i are small, (29) can be replaced by its differential equivalent

$$\ddot{x}+2h_1\dot{x}+\tilde{\omega}_1^2 x=0\ , \tag{30}$$

where

$$h_1=(8\pi)^{-1}(1-k^2) \tag{31}$$

and

$$\tilde{\omega}_1^2(\lambda)=(4\pi)^{-2}[2(k+1)-\lambda'(\lambda)]\lambda'(\lambda)\ . \tag{32}$$

$\ddot{x}$ and $\dot{x}$ denote derivatives of x taken over the continuous variable Θ, which between every other x_i changes on average by 4π. It is essential to remember that in view of the way in which Eq. (30) was obtained, it describes not the complete oscillation of the $M^{(1)}$ mode phase but only its low-frequency $\tilde{\omega}$ envelope imposed on the $\omega=\frac{1}{2}$ fast oscillation. Thus, in the vicinity of λ_1 the response of the $M^{(1)}$ mode phase to a periodic perturbation should be well approximated by

$$A(\omega,\lambda)=A(\tfrac{1}{2}-\tilde{\omega},\lambda)=C_1\{[\tilde{\omega}_1^2(\lambda)-\tilde{\omega}]^2+4h_1^2\tilde{\omega}^2\}^{-1/2}\ . \tag{33}$$

Figure 10 shows its shape for a few values of λ near λ_1.

As in the previous case the response spectrum displays a single resonance peak located at

$$\omega_{\rm res}(\lambda)=\tfrac{1}{2}-[\tilde{\omega}_1^2(\lambda)-2h_1^2]^{1/2}\ . \tag{34}$$

$\omega_{\rm res}(\lambda)$ reaches the limit $\frac{1}{2}$ value at a $\lambda_1^*<\lambda_1$ given by the condition

$$\tilde{\omega}_1^2(\lambda_1^*)=2h_1^2\ . \tag{35}$$

Thus, for $\lambda\in(\lambda_1^*,\lambda_1)$ we observe a peak located at $\omega=\frac{1}{2}$.[9] Its maximum $A(\frac{1}{2},\lambda_1-\epsilon)$ diverges near λ_1 as

$$A(\tfrac{1}{2},\lambda_1-\epsilon)=C_1(4\pi)^2\lambda_1^{-1}\epsilon^{-1}\ . \tag{36}$$

Similarly, the relaxation time τ diverges near λ_1 according to the power law

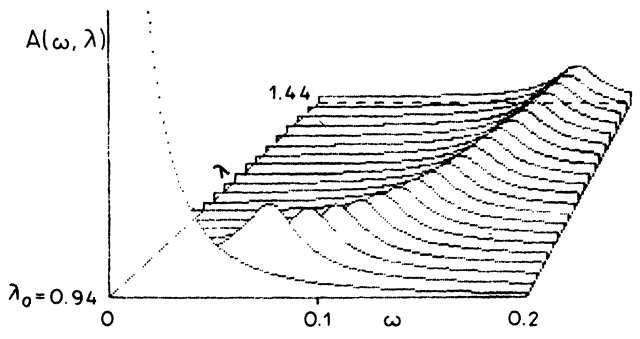

FIG. 9. Amplitude $A(\omega,\lambda)$ of the response of the $M^{(1)}$ mode phase to a periodic perturbation calculated according to (24) in the vicinity of λ_0. $k=0.85$.

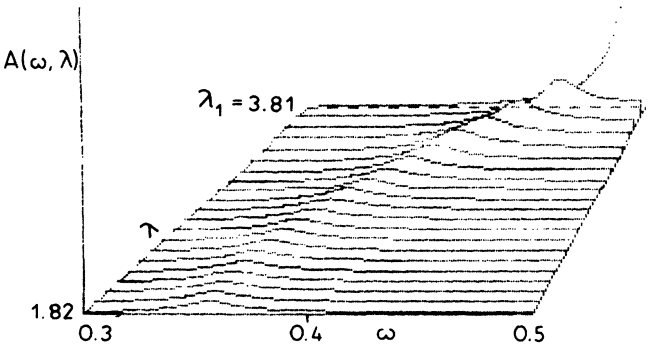

FIG. 10. Amplitude $A(\omega,\lambda)$ of the response of the $M^{(1)}$ mode phase to a periodic perturbation calculated according to (33) in the vicinity of λ_1. $k=0.85$.

$$\tau(\lambda_1-\epsilon)=4\pi(1-k^2)\lambda_1^{-1}\epsilon^{-1} . \quad (37)$$

The last result stays in agreement with what has been previously observed experimentally and confirmed by numerical calculations.[10] To check the validity of approximations (25) and (34) we performed numerical calculations which simulate the stationary spectroscopy procedure used to obtain spectra presented in Fig. 6. The simulation consisted of perturbing the surface action term $\lambda \sin\Theta$ of Eq. (6a) by a periodic signal of low amplitude γ and slowly varying frequency:

$$v_i=kv_{i-1}+\lambda \sin[\Theta_i+\gamma \sin(\tfrac{1}{2}c\Theta_i^2)] . \quad (38)$$

c was chosen such that the sweep of the perturbation frequency $\omega=c\Theta$ through the $(0,\frac{1}{2})$ range took 5×10^3 iterations. The results of the simulation are shown in Figs. 11 and 12. Figure 11 presents the position of the calculated resonant-response peak $\omega_{res}(\lambda)$ obtained at $\gamma=10^{-6}$, together with approximations (25) and (34). When the amplitude of the periodic perturbation is higher, $\gamma=10^{-2}$, $\omega_{res}(\lambda)$ changes its shape considerably, in particular near λ_1; see Fig. 12. This effect, resulting from the nonlinear response of the system, is visible also in the experimental results presented in Fig. 6. Positions of the experimental peaks, also plotted in Fig. 12, fit well the numerically determined curve.

IV. RESONANT-RESPONSE PHENOMENON AND NOISY PRECURSORS OF PERIOD-DOUBLING BIFURCATIONS

The theoretical analysis of the resonant-response phenomenon presented in Sec. III is based on Eqs. (6a) and (6b) known as the dissipative standard mapping. Consequently, results of the analysis are valid not only for the particular experimental model we designed but for all nonlinear systems whose dynamics can be described by this set of equations. On the other hand, period-doubling systems described by one-dimensional mapping are outside the validity range. In such systems, the noisy precursors of period-doubling bifurcations must occur, while the resonant-response (virtual Hopf) phenomenon need not occur.

Let us now come to the main aim of the present study, i.e., an intuitive explanation of the origin of the period-doubling noisy precursors in the nonlinear dynamical systems in which the resonant-response phenomenon occurs.

Let $M^{(\alpha)}$ be a stable periodic mode of the system described by Eqs. (6a) and (6b). The mode is represented in the power spectrum by a δ peak located at a frequency $\nu^{(\alpha)}$. On the other hand, the phase of the mode itself responds to a periodic perturbation as a damped oscillator whose resonance frequency ν_{res} changes from zero to $\nu^{(\alpha)}/2$ as the nonlinearity parameter is swept throughout the stability range of the mode. Near ends of the stability range the dynamics of the phase oscillations of the mode can formally be described in terms of conventional damped harmonic oscillators whose damping factors stay constant but whose characteristic frequencies tend to zero. Consequently, the phase of the mode becomes extremely sensitive to perturbations of well-defined frequencies:

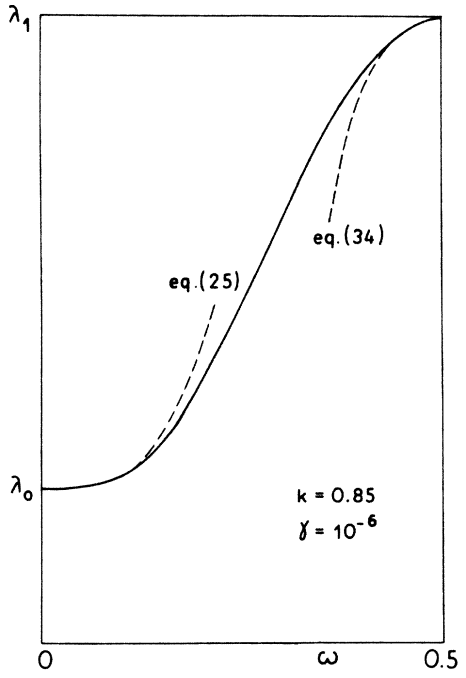

FIG. 11. Maximum response frequency $\omega_{res}(\lambda)$ of the $M^{(1)}$ mode phase calculated numerically at a low amplitude of the periodic perturbation; $\gamma=10^{-6}$. Dashed curves represent the damped harmonic oscillator approximations (25) and (34). $k=0.85$.

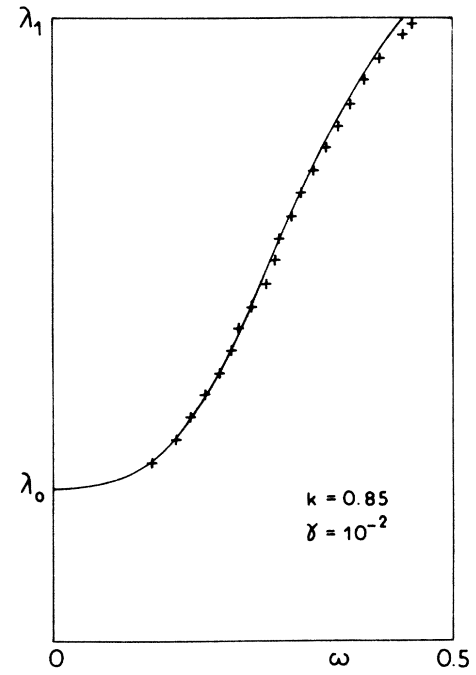

FIG. 12. Maximum response frequency $\omega_{res}(\lambda)$ of the $M^{(1)}$ mode phase calculated numerically at $\gamma=10^{-2}$. Experimental values, obtained from spectra $A,B,\ldots,W$ shown in Fig. 6, are also marked. $k=0.85$.

$\nu=0$ and $\nu=\nu^{(\alpha)}/2$ at the lower and upper stability limits, respectively. When such a system is perturbed by the white-noise signal, it will respond in a colored noisy manner. The peak in the colored noisy response spectrum will be located, of course, at the frequency ν_{res} at which the $M^{(\alpha)}$ mode phase displays its resonant behavior. According to Eqs. (27) and (36) the peak must rapidly grow near the stability limits even when because of high dissipation it was hardly visible in the middle of the stability range. This explains why for highly dissipative systems [described by the nearly one-dimensional mapping to which (6a) and (6b) reduces for $k\approx 0$] the period-doubling noisy precursors must appear while the virtual Hopf precursor (i.e., the colored response of the period-doubling mode inside its stability range) need not be visible.

On the other hand, for $k\approx 1$, i.e., when the system is nearly conservative [and mapping (6a) and (6b) nearly area preserving], the resonant-response peak should be high and sharp in the whole stability range. This may be of a practical importance since, as suggested by Wiesenfeld and McNamara,[11] period-doubling systems could be used as small-signal amplifiers. Driven by the external signal of a frequency ν_0, such systems should in the vicinity of the first period-doubling-bifurcation point provide a significant amplification of signals of $\nu_0/2$ frequency.[12] In view of the results of the present study, one may expect that the amplification should be also effective in the whole $(0,\nu_0/2)$ range, if only the nonlinear system in question was nearly conservative. In such a case the frequency ν_{res}, at which the selective amplification takes place, would be easily varied within the $(0,\nu_0/2)$ range merely by adjusting the amplitude H of the driving signal.

ACKNOWLEDGMENTS

This work has been carried out under Project MR-I.9. One of us (P.P.) would like to thank the University of Calabria, Cosenza, for financial and technical support in the experimental part of the work. We thank R. Bartolino, K. Wojciechowski, and W. Jeżewski for helpful discussions and M. Kacban for her help in numerical calculations.

[1]K. Wiesenfeld, J. Stat. Phys. **38**, 1071 (1985).
[2]C. Jeffries and K. Wiesenfeld, Phys. Rev. A **31**, 1077 (1985).
[3]P. Pierański and R. Bartolino, J. Phys. (Paris) **46**, 687 (1985).
[4]K. Wiesenfeld, Phys. Rev. A **32**, 1744 (1985).
[5]P. Pierański, J. Phys. (Paris) **44**, 573 (1983); P. J. Holmes, J. Sound Vib. **84**, 173 (1982).
[6]A. J. Lichtenberg and M. A. Lieberman, *Regular and Stochastic Motion* (Springer-Verlag, Berlin, 1983), Chap. 3; G. M. Zaslavskij, *Statistical Irreversibility in Nonlinear Systems* (Nauka, Moscow, 1970).
[7]P. Pierański, Z. Kowalik, and M. Franaszek, J. Phys. (Paris) **46**, 681 (1985).
[8]For $k=0.85$, $(\lambda_0^*-\lambda_0)/\lambda_0\approx 10^{-5}$.
[9]For $k=0.85$, $(\lambda_1-\lambda_1^*)/\lambda_1\approx 10^{-2}$.
[10]M. Franaszek and P. Pierański, Can. J. Phys. **63**, 488 (1985).
[11]K. Wiesenfeld and B. McNamara, Phys. Rev. Lett. **55**, 13 (1985).
[12]B. Derighetti *et al.*, Phys. Rev. Lett. **55**, 1746 (1985).

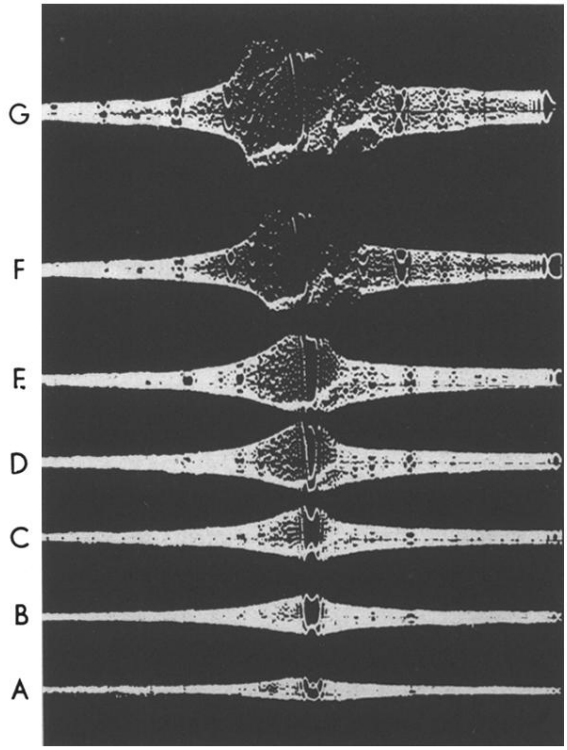

FIG. 3. Phase response spectra of the $M^{(1)}$ mode recorded for a few different amplitudes of the periodic perturbation. The amplitude H of the vibration of the collision surface determining the position of the $M^{(1)}$ mode within its bifurcation tree was the same for all presented spectra. Amplitudes of the perturbing signal were equal to 0.2, 0.3, 0.4, 0.5, 0.6, 0.75, and 1.0 for spectra denoted as $A,B,\ldots,G$. The frequency ν of the perturbing signal was swept linearly from about zero to $\nu_0/2$; $\nu_0=34$ Hz. The stroboscopic pattern of the $\frac{1}{3}$ commensurability point is clearly visible in the middle of the resonance peak.

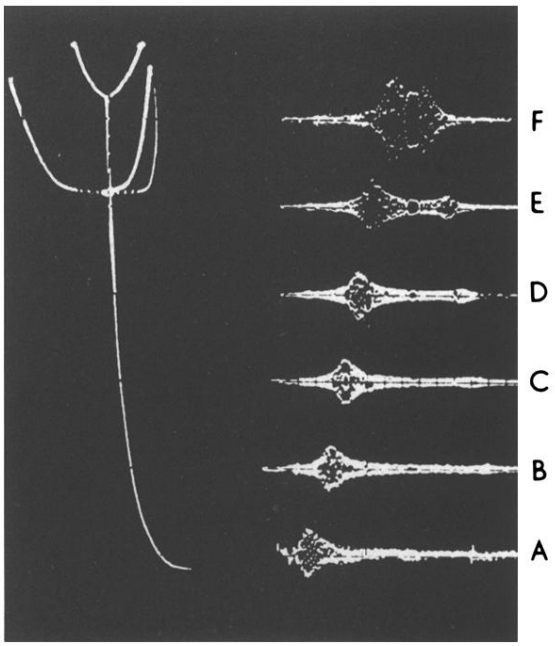

FIG. 4. Phase response FM spectra of the $M^{(1)}$ mode recorded at six points of its bifurcation tree (shown at the left side of the picture). The frequency ν of the perturbing signal was swept up to ν_0 (=33 Hz).

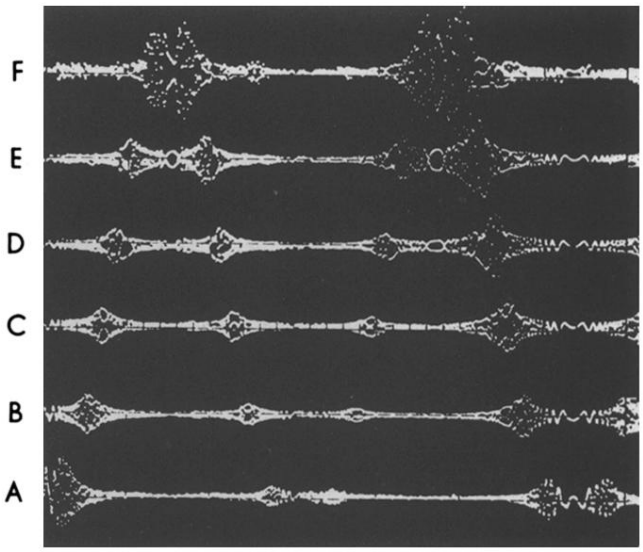

FIG. 5. Phase response AM spectra of the $M^{(1)}$ mode recorded at six points of its bifurcation tree (same as in Fig. 4). The frequency ν of the perturbing signal was swept up to $2\nu_0$ ($=33$ Hz).

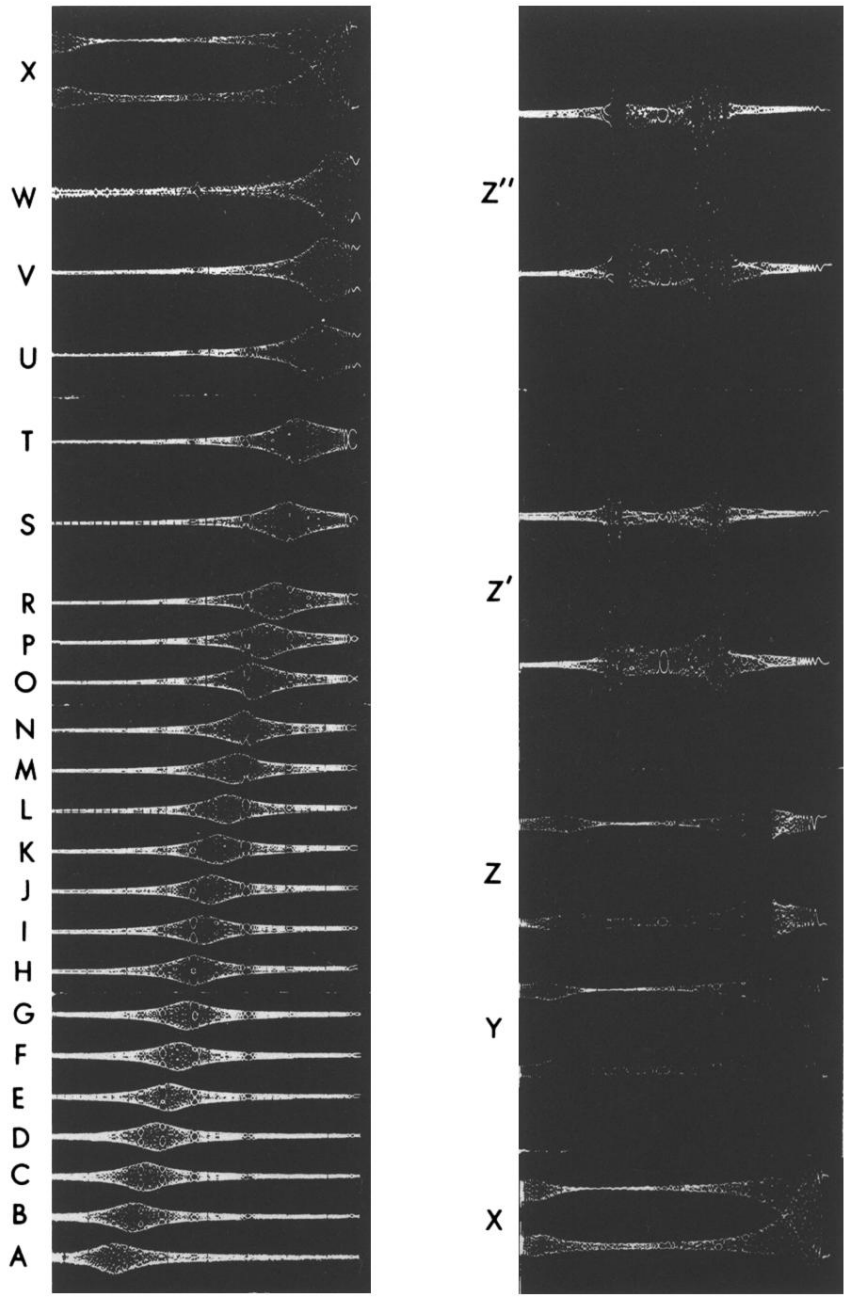

FIG. 6. Phase response FM spectra of the $M^{(1)}$ mode recorded at 27 points of its bifurcation tree including the $M^{(1,2)}$ period-doubled mode. In arbitrary units, in which $H_0=0.24$ and $H_1=1.00$, the positions of spectra indicated as $A,B,\ldots,Z,Z',Z''$ are, respectively, $H=0.28$, 0.32, 0.36, 0.39, 0.43, 0.46, 0.50, 0.54, 0.57, 0.61, 0.64, 0.68, 0.72, 0.75, 0.79, 0.82, 0.86, 0.90, 0.93, 0.97, 0.99, 1.00, 1.02, 1.04, 1.06, 1.15, 1.17. The frequency ν of the perturbing signal was swept up to $\nu_0/2$. A single frequency sweep lasted 100 s. $\nu_0=34$ Hz.

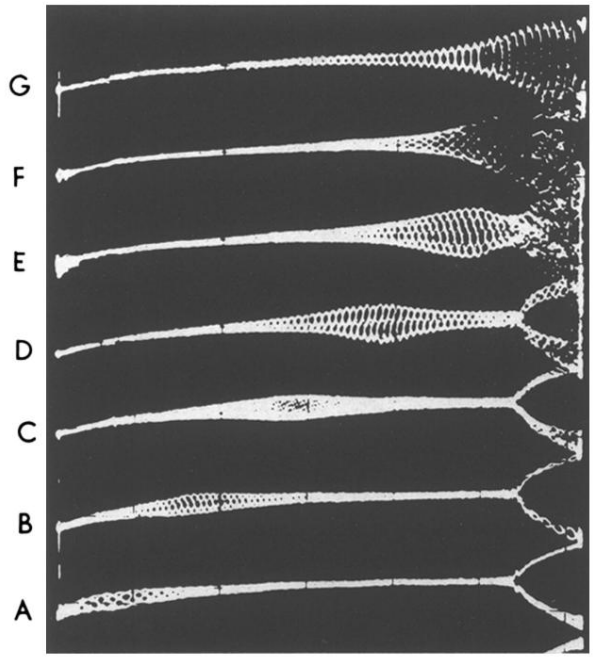

FIG. 7. Bifurcation tree of the $M^{(1)}$ mode recorded in the presence of a periodic perturbation. The frequency ν of the perturbing signal was equal to 20, 25, 30, 35, 40, 45, and 50 Hz for recordings marked, respectively, as $A,B,\ldots,G$. $\nu_0=100$ Hz.